J Mol Model (2011) 17:1941–1951
DOI 10.1007/s00894-010-0903-5

ORIGINAL PAPER

Exploration of the binding of proton pump inhibitors to human P450 2C9 based on docking and molecular dynamics simulation

Rongwei Shi · Jinyu Li · Xiaoning Cao · Xiaolei Zhu · Xiaohua Lu

Received: 31 July 2010 / Accepted: 11 November 2010 / Published online: 1 December 2010

Abstract Human P450 protein CYP2C9 is one of the major drug-metabolizing isomers, contributing to the oxidation of 16% of the drugs currently in clinical use. To examine the interaction mechanisms between CYP2C9 and proton pump inhibitions (PPIs), we used molecular docking and molecular dynamics (MD) simulation methods to investigate the conformations and interactions around the binding sites of PPIs/CYPP2C9. Results from molecular docking and MD simulations demonstrate that nine PPIs adopt two different conformations (extended and U-bend structures) at the binding sites and position themselves far above the heme of 2C9. The presence of PPIs changes the secondary structures and residue flexibilities of 2C9. Interestingly, at the binding sites of all PPI–CYP2C9 complexes except for Lan/CYP2C9, there are hydrogen-bonding networks made of PPIs, water molecules, and some residues of 2C9. Moreover, there are strong hydrophobic interactions at all binding sites for PPIs/2C9, which indicate that electrostatic interactions and hydrophobic interactions appear to be important for stabilizing the binding sites of most PPIs/2C9. However, in the case of Lan/2C9, the hydrophobic interactions are more important than the electrostatic interactions for stabilizing the binding site. In addition, an interesting conformational conversion from extended to U-bend structures was observed for pantoprazole, which is attributed to an H-bond interaction in the binding pocket, an internal π–π stacking interaction, and an internal electrostatic interaction of pantoprazole.

Keywords Docking · Molecular dynamics simulation · CYP2C9 · PPI · Binding site

Electronic supplementary material The online version of this article (doi:10.1007/s00894-010-0903-5) contains supplementary material, which is available to authorized users.

R. Shi · J. Li · X. Cao · X. Zhu (✉) · X. Lu (✉)
State Key Laboratory of Materials-Oriented Chemical Engineering, College of Chemistry and Chemical Engineering, Nanjing University of Technology,
Nanjing 210009, China
e-mail: xlzhu@njut.edu.cn

X. Lu
e-mail: xhlu@njut.edu.cn

Introduction

The cytochrome P450 (CYP or P450) enzymes, a superfamily of hemeproteins, play an important role in the metabolism of many physiologically important compounds of animals, plants, and microorganisms [1, 2]. Mammalian CYP enzymes play a central role in the detoxification of many xenobiotics such as drug molecules, environmental compounds and pollutants [3–5]. Exploring and understanding the factors involved in CYP substrate selectivity and the interaction mechanisms of CYPs with small drug molecules are interesting and challenging tasks [2], particularly for the pharmaceutical and medical industries. To obtain more information on the role of P450s in drug metabolism and their application to healthcare, a detailed knowledge of the P450 structure–function relationship [6] is essential, and will be helpful for the design and synthesis of drugs.

CYP2C9, one of the 57 currently known P450 isoenzymes [7], is one of the major enzymes responsible for phase I metabolism of drugs [7]. It is primarily embedded in the lipid bilayer of the endoplasmic reticulum of hepatocytes [8], but it also exists in other tissues including lung, kidney, and the gastrointestinal tract [9]. It accounts for the oxidative metabolism of about 16% of all

pharmaceuticals currently in clinical use, and is involved in drug interactions. Many substrates are metabolized by CYP2C9, such as anti-inflammatory agents (diclofenac [10, 11], ibuprofen [12], naproxen [13], and piroxicam [14]), anticoagulant compounds like *S*-warfarin [15, 16], and progesterone [17]. Other drugs metabolized by CYP2C9 include nonsteroidal anti-inflammatory drugs (NSAIDs) (including COX-2 selective inhibitors), the hypoglycemic agent tolbutamide, phenytoin, and the angiotensin-II receptor antagonist losartan. Inhibition of this CYP enzyme can lead to undesirable drug–drug interactions or serious drug toxicity in clinical applications [7]. Thus, it is important to investigate these inhibitors and avoid their inverse inhibitory effects or drug–drug interactions in clinical applications. To understand drug–drug interactions, we first need to elucidate the interactions of these CYPs with substrates or inhibitors. For example, the crystal structure of mammalian CYP2C9 [18, 19] has been used to predict the interactions between CYP2C9 and inhibitors.

Investigations of P450 and P450–ligand interactions have been widely performed [20]. Some nitrogen-containing heterocyclic ligands such as pyridine, imidazole, and triazole derivatives [21] have been reported to inhibit CYP enzymes by directly coordinating the heme iron [22]. The crystal structures of free CYP2C9 and CYP2C9 complexed with the anticoagulant drug warfarin were first investigated by Williams and coworkers [18]. A new binding pocket found by them indicates that CYP2C9 may simultaneously accommodate more than one ligand, which is useful for predicting potential drug–drug interactions. The metabolic sites of 14 compounds that interact with CYP2C9 have been predicted by Ahlström [7] using MetaSite [23], and the most likely docking pose for each compound has also been explored. Li et al. [24] have investigated the metabolism of gliclazide in CYP2C9 and CYP2C19 by homology modeling techniques and docking software. They used the crystal structure of CYP2C9 (PDB code: 1R9O) [19] as a template to build the CYP2C19 model. The refined homology model, which was further assessed by Profile-3D [25] and the PROCHECK software [26], was confirmed to be a reasonable model based on the docking results. Yasuo et al. [27] established a general scheme for predicting the affinities of twenty known CYP inhibitors for CYP2C9. Their results suggested that the scheme was reasonably accurate at predicting the affinities of small compounds.

So far, X-ray structures have been resolved for free CYP2C9 [18, 28] and two different substrates (*S*-warfarin [18, 28] and flurbiprofen [19]) bound to CYP2C9s and placed in the Brookhaven Protein Data Bank [29]. Proton pump inhibitors (PPIs), which have a special affinity for H^+, K^+-ATPase, are known to be the most effective agents for suppressing gastric acidity and for treating patients with acid-related diseases, such as peptic ulcer, gastroesophageal reflux disease (GERD) and Zollinger–Ellison syndrome [30]. Some PPIs (omeprazole, pantoprazole, and rabeprazole) are substituted benzimidazole sulfoxides [31, 32] and undergo extensive hepatic biotransformation [30]. As reported by Li et al. [33], some PPIs such as lansoprazole, pantoprazole, omeprazole, rabeprazole, and esomeprazole have inhibitory effects on CYP2C9. Their results suggested that pantoprazole, lansoprazole and omeprazole are the most potent inhibitors of CYP2C9 in vitro, with K_i values of 6, 21, and 15 μm, respectively. Rabeprazole and esomeprazole are weak inhibitors of CYP2C9, and their K_i values are 51 and 81 μm, respectively. To some extent, these PPIs can be metabolized by some P450 (CYP) isoenzymes in the liver [30]. Therefore, these PPIs have recently been the foci of many experimental studies [33–38]. However, the detailed mechanisms for the interaction of PPIs with CYP2C9 remain elusive. Therefore, studies on the interactions of PPIs with CYP2C9 are very important and challenging. In the present work, we use molecular docking and molecular dynamics (MD) simulation techniques to explore the structures of binding sites for PPIs/2C9 and the interaction mechanisms of PPIs with CYP2C9. At the binding sites of all PPIs/2C9 except Lan/2C9, there are interesting hydrogen-bonding networks involving PPIs, water molecules, and some residues of 2C9, which aid the stabilization of the binding sites. The present work may assist in new PPI design.

Computational methods

It is well known that there is one unbound X-ray structure of CYP2C9 (PDB code 1OG2) [18] and two structures with substrates of flurbiprofen (PDB code 1R9O) [19] and warfarin (PDB code 1OG5) [18]. The structure of 1OG5 is similar to that of 1OG2, and the difference between 1OG2 and 1R9O is that many residues are missing from the chains of 1R9O. Therefore, we choose 1OG2 as protein receptor. The structure of CYP2C9 was taken from the Brookhaven Protein Data Bank (PDB ID code: 1OG2 [18]), and its secondary structure is shown in Fig. SI-1 of the "Electronic supplementary information" (ESM). One chain of the two-chain CYP2C9 structure was focused upon in the following docking and MD simulations. As mentioned above, the substrates employed in molecular docking and MD simulations are nine proton pump inhibitors (PPIs): disuprazole (Dis), omeprazole (Ome), pantoprazole (Pan), ilaprazole (Ila), lansoprazole (Lan), rabeprazole (Rab), leminoprazole (Lem), esomeprazole (Eso), and tenatoprazole (Ten).

The coordinates of these PPIs were taken from the Drug Bank [39, 40], and these structures were optimized at the B3LYP/6-31G(d) level. Frequency analysis was then

performed, before the ESP charges were determined at the same level. All quantum chemistry calculations were realized using Gaussian 09 [41].

Docking studies were undertaken using Autodock 4.0 [42]. The Autodock program was employed to carry out automated molecule docking in order to predict the interactions of substrates with biomacromolecular targets via a number of possible search methods. Meanwhile, the atomic affinity potential for each atom type was calculated using various kinds of search algorithms, followed by rapid energy evaluation to locate appropriate binding sites for substrates on a given biomacromolecule. During the molecular docking process, CYP2C9 is kept rigid, but the positions and torsional bonds of the PPIs are set free. Polar hydrogens were added to CYP2C9. Kollman united atom partial charges were then assigned. In the grid maps calculated by AutoGrid, the chosen grid size comprised $80\times80\times94$ points with a spacing of 0.375 Å, which is sufficiently large to include most of the protein and the active sites. An empirical free-energy function and a Lamarckian genetic algorithm were employed during the process of docking the PPIs to CYP2C9. Two hundred independent runs were carried out with a maximum of 25,000,000 energy evaluations performed for each ligand. Other parameters for the genetic algorithms were not changed. When setting the docking parameters, internal electrostatic energy calculations were performed. The docking conformations were clustered according to a root-mean-square deviation (RMSD) criterion of 2.0 Å.

The MD simulations were preformed using the GROMACS package v.3.3.3 [43, 44] and the GROMOS96 force field [45, 46]. The molecular topology files for the PPIs were generated by the program PRODRG [47]. For the MD simulations, the two models (free CYP2C9, CYP2C9–PPIS complexes) were solvated with the simple point charge (SPC) water model [48]. In order to keep the systems at a constant temperature of 300 K, a Berendsen thermostat [49] was used with a coupling time of 0.1 ps. The pressure was maintained by coupling to a reference pressure of 1 bar. A coupling time of 0.5 ps was used for the simulations in bulk water [49]. The isothermal compressibility was taken to be 4.5×10^{-5} bar^{-1} for the water simulations. The LINCS algorithm [50] was used to constrain the bond lengths. Electrostatic interactions between charge groups at a distance of 9 Å were calculated explicitly. Electrostatic interactions were calculated by the particle mesh Ewald (PME) method [51]. The Lennard–Jones interactions were computed with a cutoff distance of 14 Å. For each system, the simulation cell was a rectangular box, and the minimum distance between the protein and the box walls was taken to be 10 Å. Periodic boundary conditions were applied, and the motion equations were integrated by applying the leap-frog algorithm with a time step of 2 fs. To neutralize each system, three water molecules were replaced with three Na^+ ions in free CYP2C9, or in each PPI/CYP2C9 complex. These ions were located at the positions of the oxygen atoms of waters. Finally, the simulation system for free CYP2C9 contained 4752 protein atoms and 16681 solvent molecules in a $9.3\times9.3\times6.6$ nm^3 box. Each PPI/CYP2C9 system has about 4780 solute atoms and 16680 solvent molecules embedded in a $9.3\times9.3\times6.6$ nm^3 box.

During the energy minimization of each system, the structure of the protein was fixed and all water molecules and ions in the simulations were minimized using the steepest descent method in order to satisfy the convergence criterion of 1000 kJ $mol^{-1}nm^{-1}$). A position-restrained dynamics simulation was then carried out on each system. Water molecules, proteins, and ligands were coupled separately to a temperature bath of 300 K using a coupling time of 0.1 ps. Finally, a 10 ns MD simulation was performed on each system.

Results and discussion

In our calculations, we docked the nine PPIs displayed in Fig. 1 with CYP2C9. Most of these small molecules have a benzimidazole ring, a sulfinyl group, and a pyridine ring, but they differ in their side chains. Among these PPIs, the aromatic ring of the benzimidazole structure provides the hydrophobic group, and the imidazole ring, sulfinyl group, and pyridine ring provide the negative charge centers.

The energy information obtained after docking is listed in Table SI-1 (see the "ESM"), and the binding sites of the most favorable docking structures are shown in Fig. 2. The detailed binding modes of PPIs/CYP2C9 are shown in Fig. SI-2 of the "ESM." In Fig. SI-2, amino acids that are 4 Å or closer to the PPIs are displayed. As shown in Figs. 2 and SI-2, nine PPIs position themselves inside the hydrophobic pocket formed by Phe100, Leu102, Ala103, Leu 208, Ile213, Gln214, Asn217, Asn474, Gly475, Phe476, and Ala477. The PPIs/CYP2C9 studied adopt two different binding modes, as shown in Fig. 2: (I) PPIs (Dis, Ome, Pan, and Ila) that exhibit extended geometries (Fig. 2a); (II) PPIs (Lan, Rab, Lem, Eso, and Ten) that have U-bend structures (Fig. 2(b)). The PPIs studied position themselves 10~15 Å above the heme of CYP2C9, as also described in previous results [18]. Here, the structure with >120° between the pyridine ring and the benzimidazole or an imidazopyridine ring is called the extended conformation, while the structure with two nearly parallel planes between the pyridine moiety and the benzimidazole or an imidazopyridine moiety is termed the U-bend conformation. In addition, the PPIs (except for Ila) form hydrogen bonds with adjacent residues of CYP2C9. Comparing binding mode I with binding mode II, the orientations of the benzimidiazole and pyridine groups in the PPIs are different.

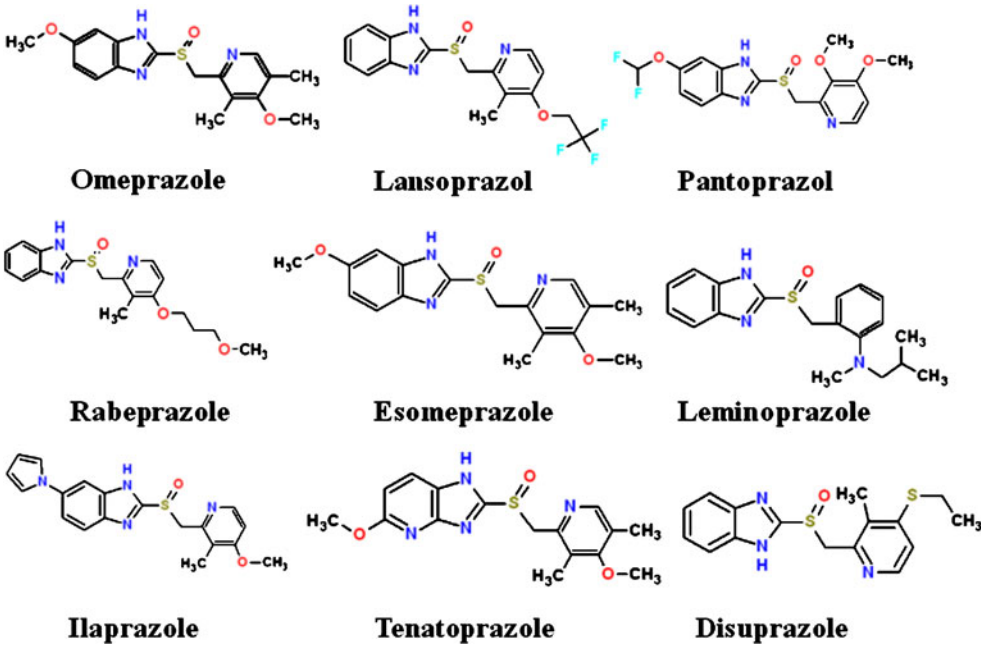

Fig. 1 Chemical structures of the PPIs included in the calculations

We use the favorable docking structures of PPIs/CYP2C9 as the initial conformations of the MD simulations. Ten-nanosecond MD simulations were then performed on these complexes to explore the dynamic properties of free CYP2C9 and PPIs/CYP2C9 complexes in water.

In order to examine whether each system stabilizes, the root-mean square deviations (RMSDs) with respect to the starting structure of the backbone C_α atoms and the total atoms for the unliganded 2C9, the liganded 2C9, and some PPIs were computed, and these are shown in Fig. 3. This figure shows that RMSD values reach stable values after about 2.5 ns for free 2C9 and most PPIs/2C9. For Ten/2C9 and Pan/2C9, the RMSD values stabilized after 8 and 8.5 ns, respectively. Figure 3b also shows that the conformation change in Rab/2C9 is relatively large, and that its RMSD values stabilize after 9 ns. It should be noted from Fig. 3c that the RMSD values for Dis and Lan tend to stabilize after 3 and 2 ns, respectively. However, for Ila, Ten, and Eso, the RMSD curves exhibit obvious changes during 5~6.5, 3.5~4.5, and 2.0~3.5 ns, respectively, and remain stable after 6.5, 4.5, and 3.5 ns, thus implying conformational changes in these PPIs.

It can be seen from Fig 4a that the total-atom RMSD of pantoprazole undergoes some changes before 3.5 ns before stabilizing at around 0.17 nm during 3.5~6.5 ns, and then increasing to ~0.28 nm. This indicates that pantoprazole undergoes conformational changes at the binding site (Fig. 4b). As shown in Fig. 4b, the planes of the benzimidazole and pyridine rings exhibit large flip-flops, and the distance and angle between benzimidazole and pyridine gradually reduce. This shows that the extended conformation gradually converts to the U-bend conformation during the simulation. The conformation with an extended or U-bend structure is characterized by particular ligand–enzyme interactions and/or internal ligand properties. For example, pantoprazole in CYP2C9 exhibits an extended structure after molecular docking, but adopts the U-bend structure after 10 ns of MD simulation due to its internal electrostatic interaction between the oxygen atom of methoxyl and the nitrogen atom of benzimidazole, the H-bond interaction in the binding pocket, and the internal π–π stacking interaction of pantoprazole.

LIGPLOT was applied to examine the hydrogen bonds and hydrophobic interactions between Dis and CYP2C9, as shown in Fig. 5a. It can be seen from Fig. 5a that there are no direct hydrogen bonds between Dis and the residues of CYP2C9. However, importantly and interestingly, the hydrogen-bond bridges of many water molecules join Dis and the residues of CYP2C9 together, as shown in Fig. 5a. For example, one strong hydrogen bond forms between the sulfinyl oxygen O11 of Dis and the water molecule W3431, and the evolution of its length over time is shown in Fig. 5b. Water molecule W3413 joins Dis and four residues (Leu208, Ser210, Gln214, Phe476) together through hydrogen bonds, which aids the stabilization of the binding site of Dis/CYP2C9. The nitrogen and oxygen atoms of Dis form four hydrogen bonds with some residues of CYP2C9 through water bridges, which may be related to the extended structure of Dis at the binding site. Figure 5b shows how the interatomic distances between "heavy" atoms associated with H-bonds evolve with time. L1 represents the distance between the oxygen O11 of Dis and the oxygen of W3431; L2 displays the distance between the oxygen of Leu208 and the oxygen of W3431; L3 indicates the distance between the

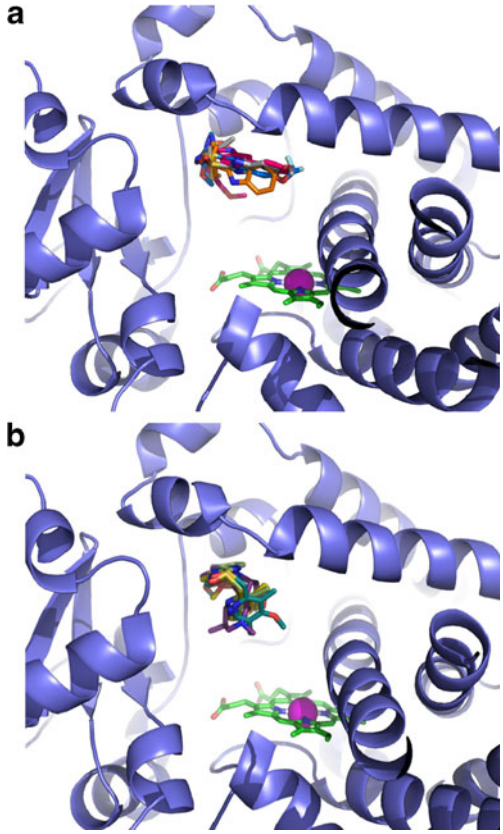

Fig. 2 **a**–**b** Most favorable docking structures of PPIs at the binding sites of PPIs/CYP2C9. **a** Binding mode I: PPIs (Dis, Ome, Pan, and Ila) exhibit extended geometries. **b** Binding mode II: PPIs (Lan, Rab, Lem, Eso, and Ten) have U-bend structures. The PPI and the heme group are shown as *sticks*. The Fe atom in the heme group is shown as a *ball*. Carbon atoms of PPIs are colored *orange* (Dis), *gray* (Ome), *sky blue* (Pan), *pink* (Ila), *yellow* (Lan), *pale yellow* (Rab), *dark green* (Eso), *purple* (Lem), and *pale green* (Ten)

amino nitrogen (NE2) of Gln214 and the oxygen of W3431; L4 represents the distance between the oxygen of Ser210 and the oxygen of W3431; L5 accounts for the distance between the amino nitrogen and the oxygen of W3431. The hydrogen-bond distances (L1~L5) stay at around 0.35 nm after 2.5 ns, which indicates that these hydrogen bonds are stable over time. Note that on the right side of Fig. 5a there are hydrophobic contacts between the benzene ring/pyridine ring of Dis and residues (Phe100, Phe69, Ile213, Pro367, and Ser209) of CYP2C9. The stabilities of the hydrophobic interactions between CYP2C9 and Dis may be estimated by examining the time dependences of the related CM distances. As shown in Fig. 5c, D1 and D2 represent the distances between the pyridine ring of Dis and the phenyl rings of Phe69 and Phe100, respectively; D3 and D4 display the distances between the phenyl ring of Dis and the main chains of Ser209 and Ile213, respectively; D5 indicates the distance from the main chain of Pro367 to the pyridine ring of Dis. Obviously, D1~D5 remain constant after 2.5 ns. These stable distances suggest that the hydrophobic interactions help to stabilize the binding site of Dis/CYP2C9. Moreover, most of the distances represented in Fig. 5b and c show significant changes before 2.5 ns and remain stable after 2.5 ns. This behavior is consistent with the results from the Cα RMSDs of the Dis/CYP2C9 complex in Fig. 3a.

Figure 6 represents snapshots of the hydrogen-bonding network at the binding site of Dis/CYP2C9 over time. It can be seen from Fig. 6 that Dis forms a weak hydrogen bond with Leu208 or Gln214 before 4 ns. Interestingly, many water molecules move into the binding site of Dis/

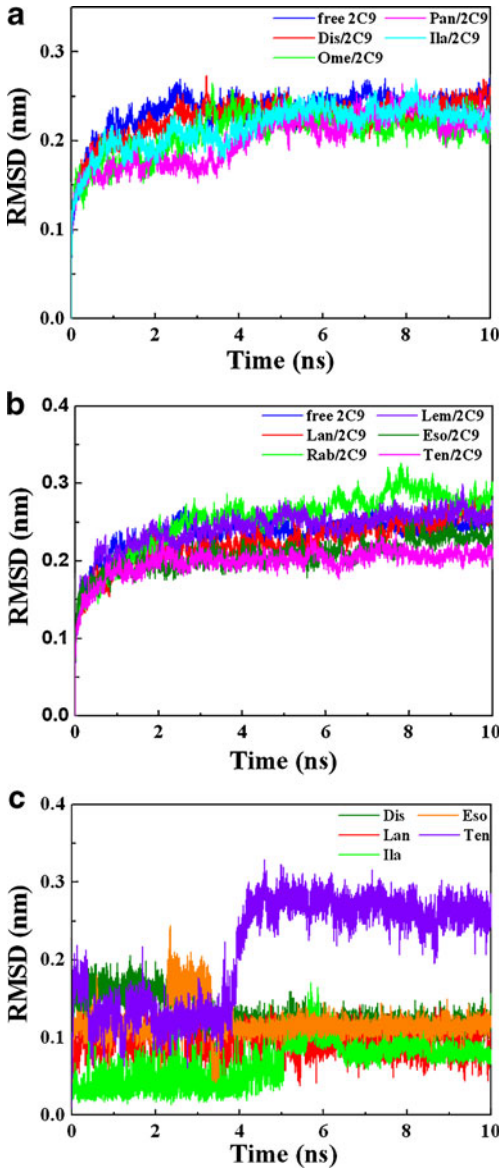

Fig. 3 **a**–**c** RMSDs from the initial structures of PPIs/CYP2C9 and some PPIs over time during MD simulations. **a** Cα RMSD for free 2C9 (*blue*), Dis/2C9 (*red*), Ome/2C9 (*green*), Pan/2C9 (*magenta*), Ila/2C9 (*cyan*). **b** Cα RMSD for free 2C9 (*blue*), Lan/2C9 (*red*), Rab/2C9 (*green*), Lem/2C9 (*purple*), Eso/2C9 (*deep green*) and Ten/2C9 (*magenta*). **c** Total-atom RMSDs for Dis (*deep green*), Lan (*red*), Ila (*green*), Eso (*orange*), and Ten (*purple*)

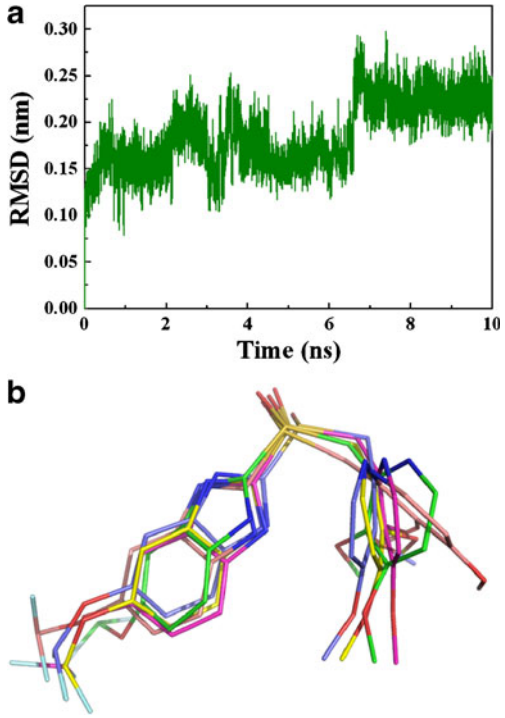

Fig. 4 **a** Total-atom RMSD of pantoprazole vs. simulation time. **b** Superposition of typical snapshots of the structure of pantoprazole after 0 ns (*brown*), 2 ns (*green*), 4 ns (*magenta*), 8 ns (*yellow*), and 10 ns (*violet*) of MD simulation

CYP2C9 during 4~10 ns. Furthermore, several water molecules in the hydrogen-bonding network always exchange with other water molecules over time, as shown in Fig. 6. It is of little surprise that water molecule W3431 always stays in the binding site and forms hydrogen bonds with the sulfinyl oxygen of Dis and the residues of CYP2C9 at 2, 4, 6, 8, and 10 ns, respectively. Clearly, the presence of these water bridges is important for stabilizing the binding site of Dis/CYP2C9. Figure SI-3 shows snapshots of the hydrogen-bonding networks, including water molecules, in the binding sites of other PPIs/CYP2C9 (except for Lan/CYP2C9) at 10 ns. In order to better understand the interactions with water in the binding pocket, the retention times for the waters that interact with Dis and its surrounding residues were estimated; these are shown in Table SI-2 of the "ESM."

However, the binding mode of Lan with CYP2C9 (shown in Fig. SI-4 in the "ESM") obtained from MD simulations is different from those of Dis/CYP2C9 and other PPIs/CYP2C9. As shown in Fig. SI-4a, there are only two hydrogen bonds between the sulfinyl oxygen of Lan and the amino N atoms of Phe476 and Ala 477, respectively. The evolutions of these two hydrogen-bond distances over time are displayed in Fig. SI-4b. L1 and L2 represent the distances between the O6 atom of Lan and the N atoms of Phe476 and Ala 477, respectively. These two

Fig. 5 **a** Two-dimensional schematic representation of hydrogen-bond and hydrophobic interactions. *W3090, W3094, W3095, W3343, W3413, W4313 and so on* represent the water molecules that form hydrogen bonds with Dis. *Dashed lines* represent hydrogen bonds, and *spiked residues* form hydrophobic interactions with Dis. The length of each hydrogen bond is given in the *middle of the dashed line*. **b** Interatomic distances associated with hydrogen-bond interactions involving Dis at the binding site of CYP2C9 versus MD simulation time. To enhance the visual clarify, the curves of L2, L3, L4 and L5 are shifted upward by 0.1, 0.2, 0.3 and 0.45 nm, respectively. **c** Center of mass distances associated with hydrophobic interactions involving Dis at the binding site of CYP2C9 versus MD simulation time. The curves of D3, D4 and D5 are shifted upward by 0.1, 0.15, and 0.25 nm, respectively

hydrogen bonds are stable during the MD simulation and have average lengths of 0.30 and 0.28 nm, respectively. Although there is no relatively stable H-bonding network in the binding site of the lansoprazole/2C9 complex, there are a few water molecules that enter the binding site and interact with lansopraole. An electrostatic interaction between the oxygen atom of methylenesulfinyl ($–CH_2SO–$) and the nitrogen atom of pyridine in lansoprazole was noted, and this may inhibit the formation of an H-bonding network between waters, lansoprazole, and residues of 2C9. Figure SI-4a also shows that there are hydrophobic contacts between the benzene ring and the pyridine ring of Lan and the residues of Leu208, Ser209, Ile213, Asn217, Phe100, and Phe114. Figure SI-4c shows how the CM distances associated with hydrophobic interactions between Lan and the residues mentioned above evolve over time. D1 represents the distance between the phenyl ring of Phe100 and the phenyl ring of Lan; D2 indicates the distance from the phenyl of Phe114 to the pyridine ring of Lan; D3 and D4 display the distances between the imidazole ring of Lan and the main chains of Leu208 and Ser209, respectively. D5 and D6 account for the distances between the phenyl rings of Lan and the main chains of Ile213 and Asn217. Clearly, the hydrophobic interactions play a relatively large role in the stabilization of the Lan/CYP2C9 binding site.

There are similar hydrogen-bonding networks in the binding sites of all PPIs/CYP2C9 complexes except Lan/CYP2C9, and water molecules enter the binding sites to interact with PPIs and residues. Although only weak hydrogen bonds form over time between some PPIs (Rab, Eso, and Lem) and residues of 2C9, other PPIs form stable hydrogen bonds with some residues of 2C9. In addition, the stronger hydrophobic interactions aid the stabilization of the binding sites of all of the PPIs/2C9 studied.

The average root-mean-square fluctuations (RMSFs) per residue (shown in Fig. SI-5 of the "ESM") are calculated from MD trajectories for unliganded and liganded CYP2C9. The larger fluctuations corresponding to the surface regions of the protein are in good agreement with B-factors for the CYP2C9 crystal structure and the simulated CYP2C9 structure from Afzelius et al. [52].

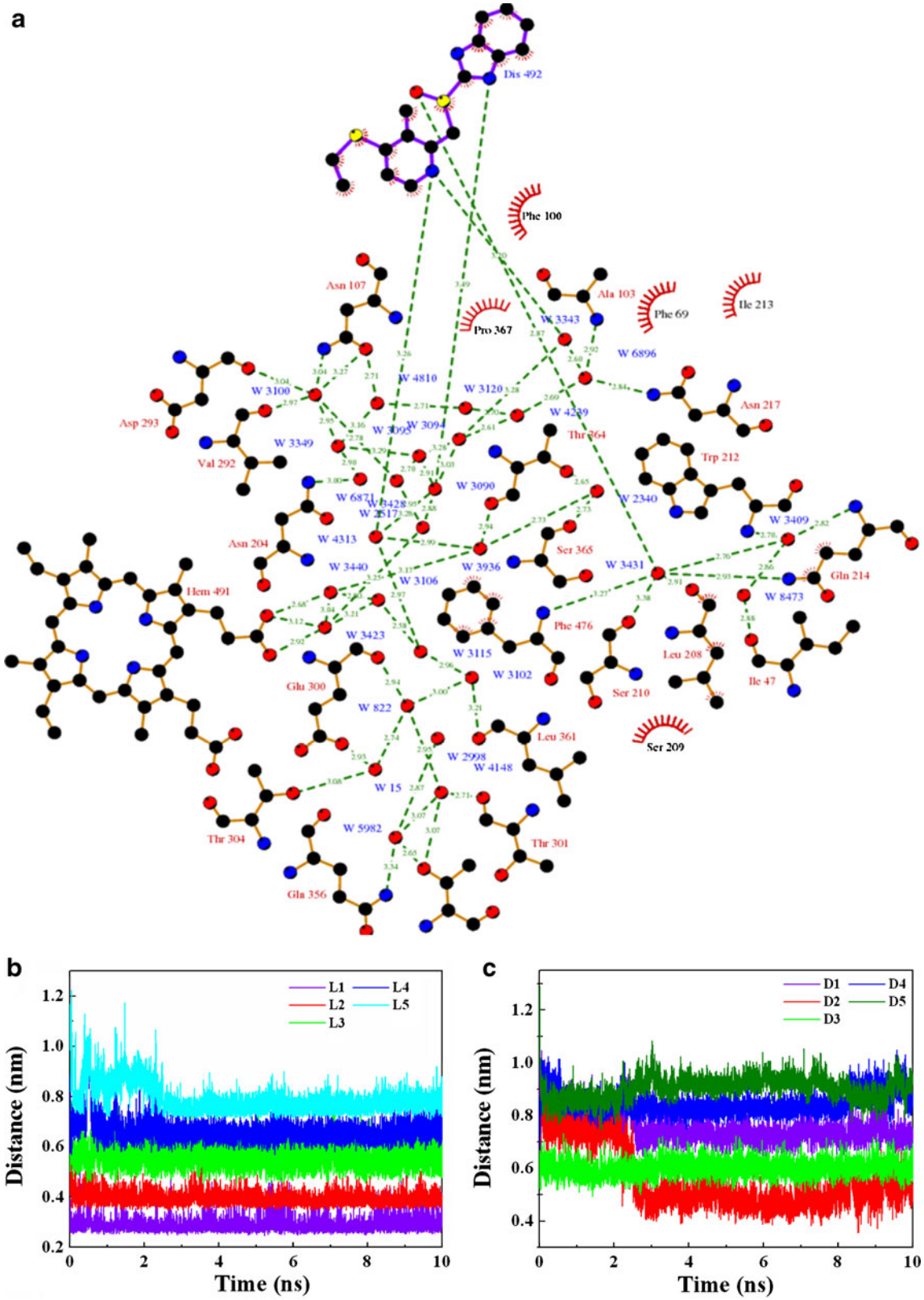
a
Dis 492
Phe 100
Asn 107
Ala 103
Phe 69
Ile 213
Pro 367
W 3343
W 6896
W 4810
W 3120
W 3100
Asn 217
Asp 293
W 4239
W 3095
W 3094
Thr 364
W 3349
Val 292
Trp 212
W 3090
W 6871
W 2340
W 3409
Asn 204
W 4313
Ser 365
W 3440
W 3936
W 3431
Gln 214
W 3106
Hem 491
W 8473
Phe 476
W 3423
Leu 208
W 3115
W 3102
Ile 47
Glu 300
Ser 210
W 822
Leu 361
Ser 209
W 2998
W 4148
W 15
W 5982
Thr 304
Thr 301
Gla 356
b
L1
L2
L3
L4
L5
Distance (nm)
Time (ns)
c
D1
D2
D3
D4
D5
Distance (nm)
Time (ns)

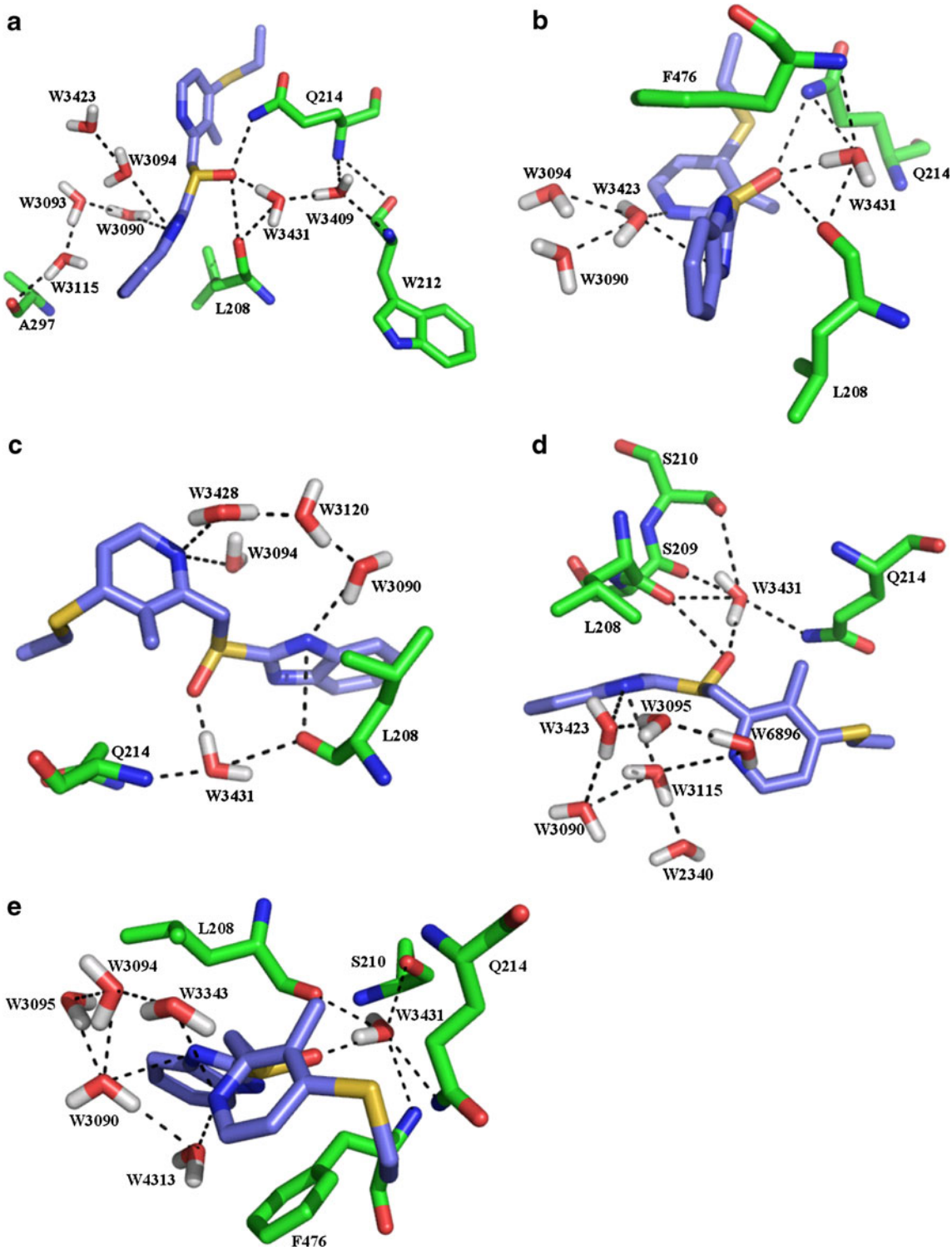

Fig. 6 **a**–**e** Snapshots of the hydrogen-bonding networks in the binding site of Dis/CYP2C9 at different simulation times: **a** 2 ns, **b** 4 ns, **c** 6 ns, **d** 8 ns, and **e** 10 ns. Carbon atoms of residues and Dis are colored in *green* and *violet*, respectively. Each *dotted line (black)* indicates a hydrogen bond

Residues with RMSFs of >0.25 nm [53] are considered highly flexible elements of CYP2C9. It can be seen from Fig. SI-5 that the RMSFs show high flexibility at the B/C loop, F/G loop, H/I loop and K/L loop regions as well as at the C-terminus for most unliganded and liganded CYP2C9. Moreover, compared with unliganded CYP2C9, the presence of PPIs significantly changes the flexibilities of some residues, as shown in Fig. SI-5.

The electrostatic potential is an effective tool that makes it possible to observe intermolecular associations and molecular properties of drug and receptor molecules [54]. Protein electrostatic properties, which play a major role in protein movement, molecular recognition and conformation flexibility, are related to polar and charged residues [55]. In order to examine the effect of electrostatic interactions on the binding sites of PPIs/CYP2C9, the electrostatic potentials of the binding sites were calculated, as shown in Fig. SI-6 in the "ESM." It can be seen in Fig. SI-6 that PPIs can form electrostatic interactions with CYP2C9 to some extent, and that these electrostatic interactions may contribute to the formation of the binding sites of PPIs/CYP2C9.

The final structures of the binding sites for Dis/2C9, Lan/2C9 and other complexes after 10 ns of MD simulation are shown in Fig. SI-7 in the "ESM." As mentioned above, in docking calculations under vacuum conditions, we obtain relatively favorable complex structures (PPIs/2C9) with binding mode I (for Dis, Ome, Pan, and Ila) and binding mode II (for Lan, Rab, Lem, Eso and Ten). During MD simulations of PPIs/2C9 in water, the presence of water and the flexibility of 2C9 can lead to conformational changes in the PPIs/2C9. It can be seen from Figs. 2 and SI-7 that the structures of most PPIs do not exhibit significant conformational changes. However, pantoprazole appears to have changed from the extended structure to the U-bend structure in the binding site, which may be due to particular ligand–enzyme interactions and internal ligand properties. The conformational change may correspond to a structure–activity relationship, although this remains to be confirmed by experiment.

The structure of ligand-free CYP2C9 has been determined to 2.6 Å resolution using a combination of the hanging-drop vapor diffusion method and molecular replacement techniques proposed by Williams et al. [18]. When CYP2C9 binds with PPIs, some parts of the protein undergo marked conformational changes; that is, the positions or the lengths of those secondary structural elements are shifted or changed relative to the corresponding structures in ligand-free CYP2C9. In order to examine the structural changes of the protein, we compared the conformations of the ligand-free CYP2C9 and the PPIs/CYP2C9 after 10 ns of simulation. Most of the PPIs/CYP2C9 and the ligand-free structures yield a very similar RMSD of 2.4 Å for all Cα atoms. However, the total Cα RMSDs for Rab/CYP2C9 and Lan/CYP2C9 are relatively large (~3.0 Å). As shown in Fig. 7, Lan-bound CYP2C9 exhibits significant conformational changes, including a structural shift, a helix length change, and a structural transition. The main conformational changes are observed in the B-C loop, the F-G region, helix E, and helix I. The hydrophobic residues (including Phe100, Phe134, Phe168, Phe226, Phe295, Phe419, Phe428, and Phe476) in most PPI/2C9 complexes exhibit some structural

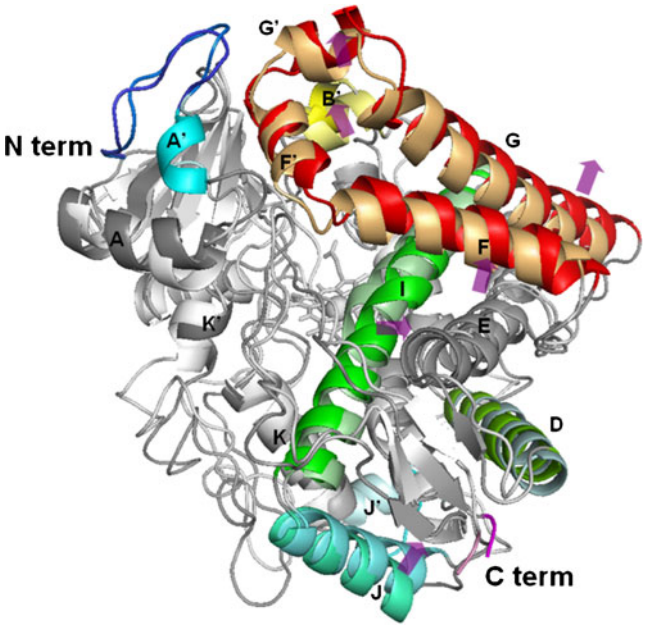

Fig. 7 Overall structures of free CYP2C9 and Lan/CYP2C9. Structures are shown in *dark gray* with helix A′ (residues 41~45) in *cyan*, helix B′ (residues 102~105) in *yellow*, helix D (residues 141~158) in *light green*, helices F to G (residues 192~253) in *red*, helix I (residues 284~315) in *green*, helix J (residues 317~330) in *teal*, helix J′ (residues 338~344) in *pale cyan*, the N-terminal loop (residues 30~40) in *blue*, and the C-terminal loop (residues 460~490) in *pink*. The structure of the complex is superposed on the ligand-free structure (Protein Data Bank ID code 1OG2), shown in *light colors*. *Violet arrows* indicate the direction of coordinate shifts in the helices B′, I and J as well as the F–G region relative to the structure of free CYP2C9

flip-flops compared with ligand-free CYP2C9 after 10 ns of simulation. Those phenyl planes on these Phe residues undergo rotations of approximately special angles (45°, 60°, 90°), and some of the hydrophobic side chains are exposed to the surrounding water. Compared with ligand-free CYP2C9, the other two parts of the secondary structural elements undergo some significant conformational changes: the coil-like residues 92–95 are changed into a helix-like structure for Ila-, Dis- and Ten-bound CYP2C9s, and the coil-like residues 161–164 are transformed into a β-sheet structure for Dis-, Eso-, Ome-, Rab-, Ten- and Lan-bound 2C9s. Some helices, such as A and G, prolong or shorten several residues by 1–3 compared with ligand-free CYP2C9. Moreover, there are distortions around residue 169 of the E helix and residue 299 of the I helix. Distortion of the I helix was also observed in the CYP3A4/ligand complex [56] and the P450eryF complex with ketoconazole [57].

Conclusions

To summarize, the binding of PPIs with 2C9 at the atomic level has been investigated and explored by docking and

MD simulations, which have revealed interesting features about this binding. PPIs exhibit two different conformations (extended and U-bend structures) at the binding site. The presence of the PPI results in secondary structural changes and changes in residue flexibility for 2C9. There are hydrogen-bonding networks for the binding sites of all PPIs/CYP2C9 complexes except Lan/CYP2C9. Water molecules enter these binding sites and join the PPIs and some residues together, which aids the stabilization of the binding sites. For lansoprazole in CYP2C9, it was found that there is an electrostatic interaction between the oxygen atom of methylenesulfinyl (–CH_2SO–) and the nitrogen atom of pyridine in lansoprazole, which may inhibit the formation of an H-bonding network. Although only weak hydrogen bonds between some PPIs (Rab, Eso, and Lem) and the residues of 2C9 evolve over time, other PPIs studied formed stable hydrogen bonds with some residues of 2C9. Moreover, there are strong hydrophobic interactions for all of the PPIs/2C9 studied that assist in the stabilization of the binding site. In addition, a change in conformation from extended to U-bend structures is observed for pantoprazole in 2C9, which may be ascribed to H-bonding at the binding site, an internal π–π stacking interaction, and an internal electrostatic interaction of pantoprazole. The current work may prove valuable in the rational design of new PPIs.

Acknowledgments This work is supported by grants from the National Science Foundation of China (nos. 20236010, 20246002, 20376032, 20706029, and 20876073), Jiangsu Science and Technology Department of China (no. BK2008372), and Nanjing University of Technology of China (no. ZK200803).

References

1. Polgár T, Menyhárd DK, Keserű GM (2007) Effective virtual screening protocol for CYP2C9 ligands using a screening site constructed from flurbiprofen and *S*-warfarin pockets. J Comput Aided Mol Des 21:539–548
2. Seifert A, Tatzel S, Schmid RD, Pleiss J (2006) Multiple molecular dynamics simulations of human P450 monooxygenase CYP2C9: the molecular basis of substrate binding and regioselectivity toward warfarin. Proteins Struct Funct Bioinf 64:147–155
3. Denisov IG, Makris TM, Sligar SG, Schlichting I (2005) Structure and chemistry of cytochrome P450. Chem Rev 105:2253–2278
4. Guengerich FP (2001) Common and uncommon cytochrome P450 reactions related to metabolism and chemical toxicity. Chem Res Toxicol 14:611–650
5. Nebert DW, Gonzalez FJ (1987) P450 genes: structure, evolution, and regulation. Annu Rev Biochem 56:945–993
6. Zhao YH, Sun L, Muralidhara BK, Kumar S, White MA, Stout DC, Halpert JR (2007) Structural and thermodynamic consequences of 1-(4-chlorophenyl)imidazole binding to cytochrome P450 2B4. Biochemistry 46:11559–11567
7. Ahlström MM, Ridderström M, Zamora I (2007) CYP2C9 structure–metabolism relationships: substrates, inhibitors, and metabolites. J Med Chem 50:5382–5391
8. Bibi Z (2008) Role of cytochrome P450 in drug interactions. Nutr Metab 5:27–36
9. Li WH, Tang Y, Liu H, Cheng J, Zhu WL, Jiang HL (2008) Probing ligand binding modes of human cytochrome P450 2J2 by homology modeling, molecular dynamics simulation, and flexible molecular docking. Proteins 71:938–949
10. Transon T, Leemann T, Vogt N, Dayer P (1995) In vivo inhibition profile of cytochrome P450TB (CYP2C9) by (±)-fluvastatin. Clin Pharmacol Ther 58:412–417
11. Poli-Scaife S, Attias R, Dansette PM, Mansuy D (1997) The substrate binding site of human liver cytochrome P450 2C9: an NMR study. Biochemistry 36:12672–12682
12. Hamman MA, Thompson GA, Hall SD (1997) Regioselective and stereoselective metabolism of ibuprofen by human cytochrome P450 2C. Biochem Pharmacol 54:33–41
13. Miners JO, Coulter S, Tukey RH, Veronese ME, Birkett DJ (1996) Cytochromes P450, 1A2, and 2C9 are responsible for the human hepatic *O*-demethylation of *R*- and *S*-naproxen. Biochem Pharmacol 51:1003–1008
14. Tracy TS, Marra C, Wrighton SA, Gonzalez FJ, Korzekwa KR (1996) Studies of flurbiprofen 4′-hydroxylation: additional evidence suggesting the sole involvement of cytochrome P450 2C9. Biochem Pharmacol 52:1305–1309
15. Rettie AE, Korzekwa KR, Kunze KL, Lawrence RF, Eddy AC, Aoyama T, Gelboin HV, Gonzalez FJ, Trager WF (1992) Hydroxylation of warfarin by human cDNA-expressed cytochrome P-450: a role for P-450 2C9 in the etiology of (*S*)-warfarin-drug interactions. Chem Res Toxicol 5:54–59
16. Thijssen HH, Flinois JP, Beaune PH (2000) Cytochrome P4502C9 is the principal catalyst of racemic acenocoumarol hydroxylation reactions in human liver microsomes. Drug Metab Dispos 28:1284–1290
17. Yamazaki H, Shimada T (1997) Progesterone and testosterone hydroxylation by cytochrome P450 2C19, 2C9, and 3A4 in human liver microsome. Arch Biochem Biophys 346:161–169
18. Williams PA, Cosme J, Ward A, Angove HC, Matak VD, Jhoti H (2003) Crystal structure of human cytochrome P450 2C9 with bound warfarin. Nature 424:464–468
19. Wester MR, Yano JK, Schoch GA, Yang C, Griffin KJ, Stout CD, Johnson EF (2004) The structure of human cytochrome P450 2C9 complexed with flurbiprofen at 2.0-Å resolution. J Biol Chem 279:35630–35637
20. Arimoto R (2006) Computational models for predicting interactions with cytochrome P450 enzyme. Curr Top Med Chem 6:1609–1618
21. Ahlström MM, Zamora I (2008) Characterization of type II ligands in CYP2C9 and CYP3A4. J Med Chem 51:1755–1763
22. Ballard SA, Lodola A, Tarbit MH (1988) A comparative study of 1-substituted imidazole and 1,2,4-triazole antifungal compounds as inhibitors of testosterone hydroxylations catalysed by mouse hepatic musomal cytochromes P-450. Biochem Pharmacol 37:4643–4651
23. Zamora I, Afzelius L, Cruciani G (2003) Predicting drug metabolism: a site of metabolism prediction tool applied to the cytochrome P450 2C9. J Med Chem 46:2313–2324
24. Yao Y, Han WW, Zhou YH, Li ZS, Li Q, Chen XY, Zhong DF (2009) The metabolism of CYP2C9 and CYP2C19 for gliclazide by homology modeling and docking study. Eur J Med Chem 44:854–861
25. Accelrys Inc. (1999) Profile-3D user guide. Accelrys Inc., San Diego
26. Laskowski RA, MacArthur MW, Moss DS, Thornton JM (1993) PROCHECK: a program to check the stereochemical quality of protein structures. Appl Crystallogr 26:283–291
27. Yasuo K, Yamaotsu N, Gouda H, Tsujishita H, Hirono S (2009) Structure-based CoMFA as a predictive model—CYP2C9 inhibitors as a test case. J Chem Inf Model 49:853–864

28. Totah RA, Rettie AE (2005) Cytochrome P450 2C8: substrates, inhibitors pharmacogenetics, and clinical relevance. Clin Pharmacol Ther 77:341–352
29. Bernstein FC, Koetzle TF, Williams GJ, Meyer EF Jr, Brice MD, Rodgers JR, Kennard O, Shimanouchi T, Tasumi M (1997) The protein data bank. A computer-based archival file for macromolecular structures. Eur J Biochem 80:319–324
30. Ishizaki T, Horai Y (1999) Review article: cytochrome P450 and the metabolism of proton pump inhibitors—emphasis on rabeprazole. Aliment Pharmacol Ther 13:27–36
31. Meyer UA (1996) Interaction of proton pump inhibitors with cytochromes P450: consequences for drug interactions. Yale J Biol Med 69:203–209
32. Nakamura M, Matsui H, Serizawa H, Tsuchimoto K (2007) Lansoprazole novel effector sites revealed by autoradiography: relation to *Helicobacter pylori*, colon, esophagus and others. J Clin Biochem Nutr 41:154–157
33. Li XQ, Andersson TB, Ahlström M, Weidolf L (2004) Comparison of inhibitory effects of the proton pump-inhibiting drugs omeprazole, esomeprazole, lansoprazole, pantoprazole, and rabeprazole on human cytochrome P450 activities. Drug Metab Dispos 32:821–827
34. Velík J, Baliharová V, Gremmels JF, Bull S, Lamka J, Skálová L (2004) Benzimidazole drugs and modulation of biotransformation enzymes. Res Vet Sci 76:95–108
35. Afzelius L, Zamora I, Masimirembwa CM, Karlén A, Andersson TB, Mecucci S, Baroni M, Cruciani G (2004) Conformer- and alignment-independent model for predicting structurally diverse competitive CYP2C9 inhibitors. J Med Chem 47:907–914
36. Masubuchi N, Li AP, Okazaki O (1998) An evaluation of the cytochrome P450 induction potential of pantoprazole in primary human hepatocytes. Chem Biol Interact 114:1–13
37. Armstrong S, Cozza KL, Benedek D (2007) Med-psych drug–drug interactions update. Psychosomatics 48:79–85
38. Ko JW, Sukhova N, Thacker D, Chen P, Flockhart DA (1997) Evaluation of omeprazole and lansoprazole as inhibitors of cytochrome P450 isoforms. Drug Metab Dispos 25:853–862
39. Wishart DS, Knox C, Guo AC, Cheng D, Shrivastava S, Tzur D, Gautam B, Hassanali M (2008) Drugbank: a knowledgebase for drugs, drug actions and drug targets. Nucleic Acids Res 36:D901–D906
40. Wishart DS, Knox C, Guo AC, Shrivastava S, Hassanali M, Stothard P, Chang Z, Woolsey J (2006) Drugbank: a comprehensive resource for in silico drug discovery and exploration. Nucleic Acids Res 34: D668–D672
41. Frisch MJ, Trucks GW, Schlegel HB, Scuseria GE, Robb MA, Cheeseman JR, Scalmani G, Barone V, Mennucci B, Petersson GA, Nakatsuji H, Caricato M, Li X, Hratchian HP, Izmaylov AF, Bloino J, Zheng G, Sonnenberg JL, Hada M, Ehara M, Toyota K, Fukuda R, Hasegawa J, Ishida M, Nakajima T, Honda Y, Kitao O, Nakai H, Vreven T, Montgomery JA Jr, Peralta JE, Ogliaro F, Bearpark M, Heyd JJ, Brothers E, Kudin KN, Staroverov VN, Kobayashi R, Normand J, Raghavachari K, Rendell A, Burant JC, Iyengar SS, Tomasi J, Cossi M, Rega N, Millam JM, Klene M, Knox JE, Cross JB, Bakken V, Adamo C, Jaramillo J, Gomperts R, Stratmann RE, Yazyev O, Austin AJ, Cammi R, Pomelli C, Ochterski JW, Martin RL, Morokuma K, Zakrzewski VG, Voth GA, Salvador P, Dannenberg JJ, Dapprich S, Daniels AD, Farkas O, Foresman JB, Ortiz JV, Cioslowski J, Fox DJ (2009) Gaussian 09, rev. A.02. Gaussian Inc., Wallingford
42. Morris GM, Goodsell DS, Halliday RS, Huey R, Hart WE, Belew RK, Olson AJ (1998) Automated docking using a Lamarckian genetic algorithnm and an empirical binding free energy function. J Comput Chem 19:1639–1662
43. Berendsen HJC, van der Spoel D, van Drunen R (1995) GROMACS: a message-passing parallel molecular dynamics implementation. Comput Phys Commun 91:43–56
44. Lindahl E, Hess B, van der Spoel D (2001) GROMACS 3.0: a package for molecular simulation and trajectory analysis. J Mol Model 7:306–317
45. van der Spoel D, van Buuren AR, Peter Tieleman D, Berendsen HJC (1996) Molecular dynamics simulations of peptides from BPTI: a closer look at amide–aromatic interactions. J Biomol NMR 8:229–238
46. Hermans J, Berendsen HJC, van Gunsteren WF, Postma JPM (1984) A consistent empirical potential for water–protein interactions. Biopolymers 23:1513–1518
47. van Aalten DMF, Bywater R, Findlay JBC, Hendlich M, Hooft RWW, Vriend G (1996) PRODRG, a program for generating molecular topologies and unique molecular descriptors from coordinates of small molecules. J Comput-Aided Mol Des 10:255–262
48. Fuhrmans M, Sanders BP, Marrink SJ, de Vries AH (2010) Effects of bundling on the properties of the SPC water mode. Theor Chem Acc 125:335–344
49. Berendsen HJC, Postma JPM, van Gunsteren WF, DiNola A, Haak JR (1984) Molecular dynamics with coupling to an external bath. J Chem Phys 81:3684–3690
50. Hess B, Bekker H, Berendsen HJC, Fraaije JGEM (1997) LINCS: a linear constraint solver for molecular simulations. J Comput Chem 18:1463–1472
51. Darden T, York D, Pedersen L (1993) Particle mesh Ewald: an N·log(N) method for Ewald sums in large systems. J Chem Phys 98:10089–10092
52. Afzelius L, Raubacher F, Karlén A, Jørgensen FS, Andersson TB, Masimirembwa CM, Zamora I (2004) Structural analysis of CYP2C9 and CYP2C5 and an evaluation of commonly used molecular modeling techniques. Drug Metab Dispos 32:1218–1229
53. Gajendrarao P, Krishnamoorthy N, Sakkiah S, Lazar P, Lee KW (2010) Molecular modeling study on orphan human protein CYP4A22 for identification of potential ligand binding site. J Mol Graph Model 28:524–532
54. Sinha N, Smith-Gill SJ (2002) Electrostatics in protein binding and function. Curr Protein Pept Sc 3:601–614
55. Weiner PK, Langridge R, Blaney JM, Schaefer R, Kollman PA (1982) Electrostatic potential molecular surfaces. Proc Nat Acad Sci USA 79:3754–3758
56. Ekroos M, Sjögren T (2006) Structural basis for ligand promiscuity in cytochrome P450 3A4. Proc Nat Acad Sci USA 103:13682–13687
57. Cupp-Vickery JR, Garcia C, Hofacre A, McGee-Estrada K (2001) Ketoconazole-induced conformational changes in the active site of cytochrome P450eryF. J Mol Biol 311:101–110